

# We are IntechOpen, the world's leading publisher of Open Access books Built by scientists, for scientists

6,900

Open access books available

186,000

International authors and editors

200M

Downloads

Our authors are among the

154

Countries delivered to

TOP 1%

most cited scientists

12.2%

Contributors from top 500 universities



WEB OF SCIENCE™

Selection of our books indexed in the Book Citation Index  
in Web of Science™ Core Collection (BKCI)

Interested in publishing with us?  
Contact [book.department@intechopen.com](mailto:book.department@intechopen.com)

Numbers displayed above are based on latest data collected.  
For more information visit [www.intechopen.com](http://www.intechopen.com)



---

# Applications of Nano-Scale Plasmonic Structures in Design of Stub Filters — A Step Towards Realization of Plasmonic Switches

---

Hassan Kaatuzian and Ahmad Naseri Taheri

Additional information is available at the end of the chapter

<http://dx.doi.org/10.5772/59877>

---

## 1. Introduction

As electronic devices and circuits were shrinking to the nano-scale chips, some drawbacks hindered the reaching to the speed higher than tens of Giga Hertz, such as the higher power consumption, delay, and interference of the signals. However, the need for transmitting the huge amount of data over communication networks urged everyone in this area of technology to find an alternative for pure electronic devices. Despite rapidly developing the photonics technology, in practice the implementation of the photonic counterparts of the electronic devices encountered many problems such as inability to become integrated. The size of photonic devices halted on the half the wavelength of the operating signal due to the Diffraction limit of light.

In recent years, Surface Plasmon Polaritons (SPPs) have been considered as one of the most promising ways to overcome the diffraction limits of photonic devices. The field of manipulating the SPPs as the carrier of the signal is known as Plasmonics. In plasmonics, the advantages of electronics such as nano-scale component design are joint together with the benefits of photonics. Therefore, plasmonics shapes a key part of the fascinating field of nanophotonics, which discovers how electromagnetic fields can be confined over dimensions on the order of or smaller than the wavelength. It is constructed based on interaction of electromagnetic radiation and conduction electrons at metallic interfaces or in small metallic nanostructures, leading to enhance the confinement of optical field in a sub-wavelength dimension.

The strong interaction between microscopic metal particles and light has been utilized for thousands of years, the Lycurgus Roman Cup dating from 4<sup>th</sup> century A.D. [1], brightly colored stained-glass window panels by annealing metallic salts in transparent glass [1]. The practical instructions for this ancient “nanofabrication” technique survive from as early as the

8th century A.D. [1]. From the beginning of the 20<sup>th</sup> century many phenomena related to the unusual optical properties of particles and spheres were explained; the blue color of the sky in terms of a simple derivation of the scattering power of spheres by Rayleigh [2], the bright color of metal glass by Garnett [3], presentation of a general formulation for the scattering of light from spherical surface by Gustav Mie [4]. In 1957, Ritchie [5] described surface plasmons in thin films in terms of electron energy loss spectroscopy. Otto [6], Kretschmann and Raether [7] explained the procedures for exciting surface plasmons on thin films optically in 1968. In 1974, the enhancement of Raman scattering from molecules influenced by the enhanced local fields at a rough metal surface was first observed by Fleischmann et al. [8].

In recent years, the applications of the surface plasmons are extended in optical integrated circuits and create a rapid developing field of photonics known as Plasmonics. Many researches are being carried out on developing plasmonic structures. Plasmonic switches and modulators are the most important components used for light routing and switching in the rapidly developing area of broadband optical communications and designing ultra-high speed switching devices, where sub-femtosecond interaction of light with matter is our main design concern [9]. Numerous plasmonic devices and components are introduced and huge of research are published. By exciting of the surface plasmons at the boundary of dielectric and metallic materials, an optical field can be confine into a subwavelength dimension [10]. A plasmonic circuit transforms the light into surface plasmons at the same frequency but reduced dimensions, in addition to guidance that is more flexible and highest speed.

In the next section of this chapter, Metal-Optics Electromagnetism is discussed. In section 3, wave analysis is used for explaining the propagation of surface plasmon polaritons. Section 4 is dedicated to investigate the various schemes of plasmonic guiding and their characteristics. In section 5, the modeling methods of plasmonic waveguides are introduced, and in section 6, a case study of plasmonic application in designing a switch is presented.

## 2. Metal-optics electromagnetism

Surface plasmons polaritons (SPPs) are surface electromagnetic modes that propagate at the interface of a dielectric with real electric permittivity  $\epsilon_1$  and a metal with permittivity  $\epsilon_2(\omega) < 0$  as shown in figure 1.

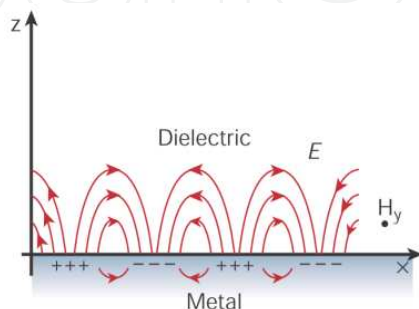


**Figure 1.** Electric and magnetic field distributions and charge oscillations at the dielectric/metal interface. SPPs propagate along the x-direction.

The complex permittivity or complex dielectric function can be expressed as [11]:

$$\varepsilon = \varepsilon' + i\varepsilon'' \quad (1)$$

where  $\varepsilon'$  is the real part and  $\varepsilon''$  is the imaginary part of the permittivity. In addition, the response of the material to the incoming optical field is expressed as the complex refractive index as [12]:

$$N = n + ik \quad (2)$$

where  $n$  and  $k$  are the real and imaginary part of the refractive index. The equations (1) and (2) are related to each other by:

$$\varepsilon' = n^2 - k^2 \quad (3)$$

$$\varepsilon'' = 2nk \quad (4)$$

These parameters are known as optical constants of the material however, in many of the materials they change with the frequency of the incident optical field. Especially in metals, the dielectric parameters are strongly dependent to the optical frequency. In order to use the permittivity of metals in the calculations of the spectrometry some mathematical models are introduced, such as Lorentz model, Lorentz-Drude model and Extended Drude model.

### 2.1. Lorentz model

In plasmonic, the optical properties of material can be expressed as a classical physical model of the microscopic structure [3], in which the charge carriers are assumed as damped harmonic oscillators subjected to incident electromagnetic field as driving forces. In the Lorentz model a charge carrier is supposed to have a mass of  $m$ , charge  $e$  and displacement from equilibrium  $x$ . The force on this particle as a linear spring force is  $F = K \cdot x$ , the velocity dependent damping is  $F = b \cdot \dot{x}$  and the driving force by any incident light is  $F = eE$ . Therefore, the equation of motion is [12, 13]:

$$m\ddot{x} + b\dot{x} + Kx = eE \quad (5)$$

normalizing the above equation by mass:

$$\ddot{x} + \gamma + \omega_0^2 x = \frac{e}{m} E \quad (6)$$

where  $\omega_0^2 = K/m$  and  $\gamma = b/m$ . By solving the equation (6) as a time-harmonic and substitution of  $\dot{x} \leftrightarrow -i\omega x$  and  $\ddot{x} \leftrightarrow -\omega^2 x$ :

$$x = \frac{\left(\frac{e}{m}\right) \mathbf{E}}{\omega_0^2 - \omega^2 - i\gamma\omega} \quad (7)$$

Supposing  $N$  particles per volume  $V$  and dipole  $p = ex$  for each particle, the polarization is  $\mathbf{P} = \left(\frac{N}{V}\right)p$ . Therefore, equation (7) can be expressed:

$$\mathbf{P} = \frac{\omega_p^2}{\omega_0^2 - \omega^2 - i\gamma\omega} \varepsilon_0 \mathbf{E} \quad (8)$$

where  $\omega_p$  is the plasma frequency and is defined as:

$$\omega_p^2 = \frac{\left(\frac{N}{V}\right)e^2}{m\varepsilon_0} \quad (9)$$

From the Maxwell's equation, we have:

$$\varepsilon = 1 + \chi \quad (10)$$

$$\mathbf{P} = \varepsilon_0 \chi \mathbf{E} \quad (11)$$

Therefore, from the equations (8), (10) and (11) the Lorentz model for the dielectric function is derived:

$$\varepsilon_{\text{Lorentz}}(\omega) = 1 + \frac{\omega_p^2}{\omega_0^2 - \omega^2 - i\gamma\omega} \quad (12)$$

## 2.2. Multi-oscillator Drude-Lorentz model

Here, the model is the superposition of  $j+1$  individual oscillators [12]:

$$\varepsilon_{\text{Drude-Lorentz}}(\omega) = 1 - \frac{f_0 \omega_{p,0}^2}{\omega^2 + i\gamma_0 \omega} + \sum_{j=1}^{j_{\max}} \frac{f_j \omega_{p,j}^2}{\omega_j^2 - \omega^2 - i\gamma_j \omega} \quad (13)$$

where  $f_j$ 's are the oscillator strengths,  $\omega_{p,j}$ 's are the plasma frequencies,  $\gamma_j$ 's are damping rates and  $\omega_j$ 's are the oscillator frequencies. The second term of equation (13) is the Drude term

and represents the free electrons, which are not under the restoring force. Using 5 terms of the Lorentz model constructs an excellent approximation of optical properties of metals and many semiconductors in the visible spectrum [12].

### 3. Wave approach for the propagation of the surface plasmon polaritons

Surface plasmon polaritons are electromagnetic waves propagating at the interface between a dielectric and a metal evanescently bounded in the perpendicular direction [4]. These electromagnetic surface waves are created from the coupling of the optical fields to oscillations of the metal's electron plasma. Based on the dispersion relation and the spatial field distribution, the surface plasmons are described quantitatively.

#### 3.1. Propagating the SPPs at a single metal-insulator interface

##### 3.1.1. Deriving the dispersion relation

By solving the Maxwell's equation at a single metal-insulator interface, the wave equation is produced, in which for the transverse magnetic (TM or p) modes is [14]:

$$\frac{\partial^2 H_y}{\partial z^2} + (k_0^2 \varepsilon - \beta^2) H_y = 0 \quad (14)$$

and for transverse electric (TE or s) modes is:

$$\frac{\partial^2 E_y}{\partial z^2} + (k_0^2 \varepsilon - \beta^2) E_y = 0 \quad (15)$$

where  $k_0 = \omega / c_0$  is the wave vector of the propagating wave in vacuum. Now, we should consider a simple flat boundary between an insulator ( $z > 0$ ) with a real positive permittivity  $\varepsilon_2$  and a metal ( $z < 0$ ) with a complex permittivity  $\varepsilon_1(\omega)$  (for metals  $Re\{\varepsilon_1(\omega)\} < 0$ ). Supposing the condition of propagating wave bounded to the interface with evanescent falloff in z-direction, the solutions for TM waves in  $z > 0$  is [14]:

$$H_y(z) = A_2 e^{i\beta x} e^{-k_2 z} \quad (16)$$

$$E_x(z) = iA_2 \frac{1}{\omega \varepsilon_0 \varepsilon_2} k_2 e^{i\beta x} e^{-k_2 z} \quad (17)$$

$$E_z(z) = -A_1 \frac{\beta}{\omega \varepsilon_0 \varepsilon_2} k_2 e^{i\beta x} e^{-k_2 z} \quad (18)$$

and for  $z < 0$  is:

$$H_y(z) = A_1 e^{i\beta x} e^{k_1 z} \quad (19)$$

$$E_x(z) = -iA_1 \frac{1}{\omega \varepsilon_0 \varepsilon_1} k_1 e^{i\beta x} e^{k_1 z} \quad (20)$$

$$E_z(z) = -A_1 \frac{\beta}{\omega \varepsilon_0 \varepsilon_1} k_2 e^{i\beta x} e^{k_1 z} \quad (21)$$

where  $k_i \equiv k_{z,i}$  is the component of the wave vector at  $z$ -direction. The reciprocal value of the  $k_i$ ,  $\hat{z} = 1 / |k_z|$ , is evanescent decay length of the fields in the perpendicular of the propagation [14].

The continuity condition of  $H_y$  and  $\varepsilon E_z$  at the interface implies that  $A_1 = A_2$  and

$$\frac{k_2}{k_1} = -\frac{\varepsilon_2}{\varepsilon_1} \quad (22)$$

Because at the interface of insulator and metal  $Re\{\varepsilon_2\} > 0$  and  $Re\{\varepsilon_1\} < 0$  the propagating waves confines at the surface. Based on equation (14) for TM waves at metal and insulator [14],

$$k_1 = \beta^2 - k_0^2 \varepsilon_1 \quad (23)$$

$$k_2 = \beta^2 - k_0^2 \varepsilon_2 \quad (24)$$

Therefore, by combining the equations (22), (23) and (24), the dispersion relation of the SPPs propagating at the metal-insulator yields

$$\beta = k_0 \sqrt{\frac{\varepsilon_1 \varepsilon_2}{\varepsilon_1 + \varepsilon_2}} \quad (25)$$

### 3.1.2. Forbidden modes for surface plasmons

Based on equation (15), the field components for TE modes are

$$E_y(z) = A_2 e^{i\beta x} e^{-k_2 z} \quad (26)$$

$$H_x(z) = -iA_2 \frac{1}{\omega\mu_0} k_2 e^{i\beta x} e^{-k_2 z} \quad (27)$$

$$H_z(z) = A_2 \frac{\beta}{\omega\mu_0} k_2 e^{i\beta x} e^{-k_2 z} \quad (28)$$

for  $z > 0$ , and

$$E_y(z) = A_1 e^{i\beta x} e^{k_1 z} \quad (29)$$

$$H_x(z) = iA_1 \frac{1}{\omega\mu_0} k_1 e^{i\beta x} e^{k_1 z} \quad (30)$$

$$H_z(z) = A_1 \frac{\beta}{\omega\mu_0} e^{i\beta x} e^{k_1 z} \quad (31)$$

In calculations of the equations (26) to (31), the following equations are used:

$$H_x = i \frac{1}{\omega\mu_0} \frac{\partial E_y}{\partial z} \quad (32)$$

$$H_z = \frac{\beta}{\omega\mu_0} E_y \quad (33)$$

From the continuity of  $E_y$  and  $H_x$  at the interface

$$A_1(k_1 + k_2) = 0 \quad (34)$$

and because of the confinement condition requires  $Re\{k_1\} > 0$  and  $Re\{k_2\} > 0$ , hence  $A_1 = 0$  and  $A_2 = 0$ ; therefore, there are no TE modes at the surface. That means, the surface plasmon polaritons propagate only in TM polarization [14].

### 3.1.3. Propagation Length of SPPs

An important parameter in comparing plasmonic waveguide structures is the **propagation length** of a supported mode. As a surface plasmon propagates along the surface, it quickly loses its energy to the metal due to absorption. The intensity of the surface plasmon decays with the square of the electric field, so at a distance  $x$ , the intensity has decreased by a factor of  $\exp(2\text{Im}(\beta_z)z)$  [15]. The propagation length is defined as the distance for the surface plasmon to decay by a factor of  $1/e$ . This condition is satisfied at a length

$$L_{SPP} = \frac{1}{2\text{Im}(\beta_z)} \quad (35)$$

The typical value for propagation length in plasmonic metal-insulator waveguides is up to  $100\mu\text{m}$  in visible regime [14].

## 4. Plasmonic waveguide schemes

The fundamental element in integrated plasmonic circuitry, as in photonics, is the waveguide. Because the necessity of existence of metal layer and various structural possibilities of using metal layer, many of schemes are developed in the recent years [11]. Each of the schemes has some benefits and drawbacks, in which make a trade-off between their characteristics. Two main characteristics of a waveguide are the confinement area of the mode and the propagation length. This features of the plasmonic waveguides are in opposite and there are a trade-off between them.

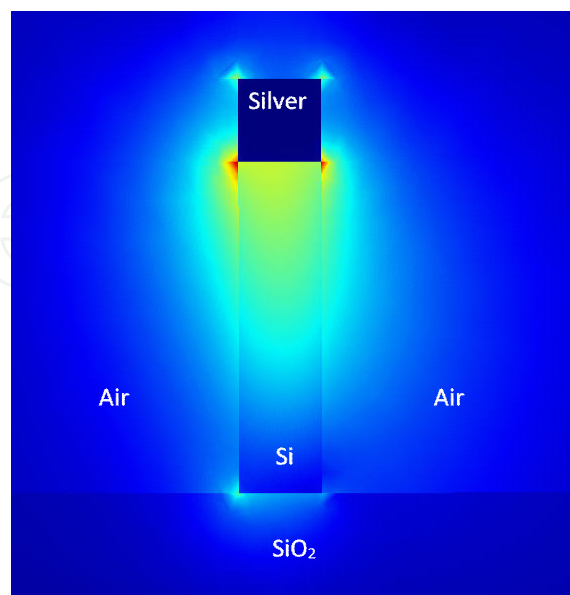


**Figure 2.** Optical field distribution at cross section of insulator-metal waveguide

In this section, some of the well-known types of plasmonic waveguides structures will be briefly introduced. In each case, the advantage(s) and weakness(s) of the waveguide are investigated.

#### 4.1. Insulator-Metal (IM) waveguide

The simplest structure for guiding the plasmon polaritons is the Insulator-Metal (IM) waveguide (figure 2). This scheme consists a thin film metal coated on a simple insulator strip waveguide [11]. The silicon core of the waveguide has dimension about  $300\text{nm} \times 300\text{nm}$  and the cladding of the waveguide is the air. The metal cap has a  $50\text{nm}$  thickness and can be gold or silver. The structure placed on a  $\text{SiO}_2$  substrate. The propagation length of this fundamental scheme is  $2\mu\text{m}$  at  $1550\text{nm}$  [11]. In this structure, a relative good balance exists between propagation length and confinement. In addition, the material used in fabrication allows feasibility of integrated plasmonic circuitry [11].

#### 4.2. Dielectric-loaded SPP waveguide

The dielectric-loaded SPP waveguides (DLSPWs) are formed by placing a polymethylmethacrylate (PMMA) ridge with a cross section of  $500\text{ nm}$  in width by  $600\text{ nm}$  in height as the dielectric material on top of a  $65\text{ nm}$  thick and  $3\mu\text{ m}$  wide gold strip [16] (figure 3a). This scheme provides a full confinement in the plane perpendicular to the propagation direction. This geometry is one of the most popular for plasmonic waveguides because PMMA can work as both resist and the dielectric core for the DLSPW [16]. There is a convenient and simple process to fabricate plasmonic devices based on DLSPW using deep-ultraviolet (UV) lithography for those devices with larger dimensions working at telecom wavelengths or standard E-beam lithography (EBL) for those working in the near-infrared. In addition, due to the physical dimension and therefore the mode size increase, this structure has slightly better propagation length for SPP's going from  $5\mu\text{ m}$  to  $25\mu\text{ m}$ .

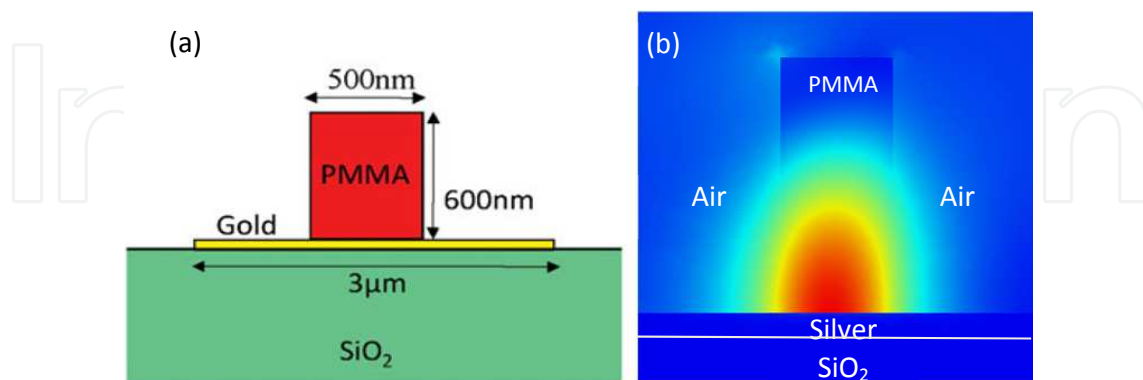


**Figure 3.** (a) Schematic representation of the DLSPW cross section [16]. (b) Mode distribution of DLSPW of optimal configuration.

Compared with other waveguide schemes, DLSPWs are well-matched with different dielectrics and have a rather good trade-off between mode confinement and propagation

distance [16]. These characteristics make them suitable for realization of dynamic components by utilizing of material (e.g., thermo- and electro-optic) effects, while strong mode confinement and long propagation distances are required for realization of compact and complex plasmonic circuits [16].

#### 4.2.1. Long-Range Dielectric-Loaded Surface Plasmon Polaritons waveguides (LR-DLSPPs)

The long-range plasmonic waveguide is, unlike previous studies of DLSPPWs, based on a metal film with finite width [17], i.e., a metal strip, and can thus be considered a hybrid plasmonic waveguide (discussed later). The LR-DLSPPW configuration consists of a dielectric ridge placed on top of a thin metal strip, which is supported by a dielectric film (figure 4a). The entire structure is supported by a low-index substrate that ensures mode confinement to the dielectric ridge and underlying dielectric film [17].

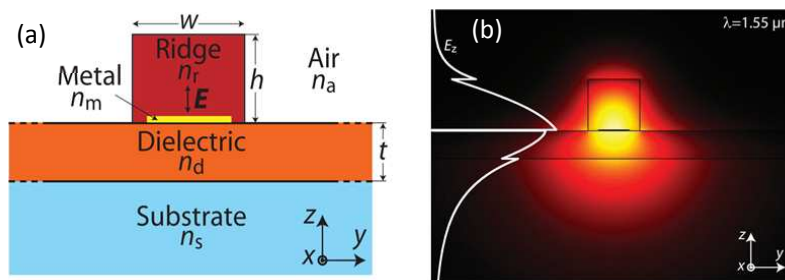


**Figure 4.** (a) Layout of the LR-DLSPPW structure, with a dielectric ridge on top of a thin metal stripe deposited on an underlying dielectric layer supported by a low-index glass substrate, (b) optical field distribution in the cross-section of the LR-DLSPPW [17].

Because of varying the thickness of the PMMA layer and hence, balancing the mode field on either side of the metal strip (figure 4b), this structure minimizes the losses and increase the propagation length to  $L = 3100\mu\text{m}$ , while retaining strong mode confinement [17].

### 4.3. Hybrid plasmonic waveguide

As a solution to the issue of propagation loss of SPPs, a new waveguide known as hybrid plasmonic waveguide (HPWG) is presented [18]. Figure 5a shows the cross section of a two dimensional HPWG. It consists of a high index region (silicon) disjointed from a silver surface by a low index layer ( $\text{SiO}_2$ ). The close area of the silver-silica interface and the silicon slab results in coupling of the SPP mode and dielectric waveguide mode supported by these two structures. Figure 5b shows the resulting hybrid mode. The guide also supports a conventional TE mode, which is shown in figure 5c. The mode sizes for both TE and TM modes are comparable in this case and are very similar to mode size achievable in case of silicon waveguide. HPWG offers a number of benefits [18]: it has an improved compromise between loss and confinement compared to purely plasmonic waveguides, and is compatible with silicon on insulator technology. The power of the TE and TM modes in the HPWG are concentrated in two different layers, therefore their guiding characteristics can be controlled in different manners by altering the material properties, and waveguide dimensions of the layers [18].

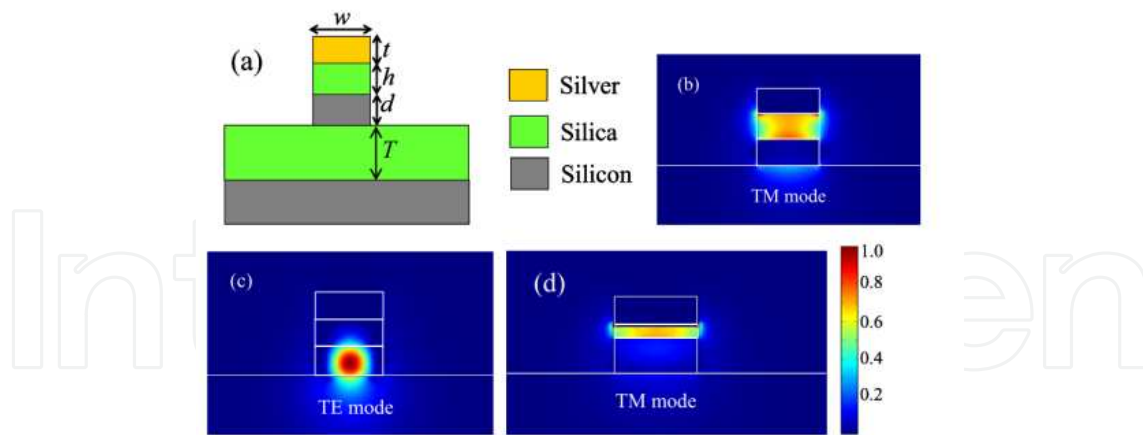


**Figure 5.** (a) Schematic of a hybrid waveguide. (b) and (c) power density profile for the TM and TE modes respectively for waveguide dimensions are  $w = 350$  nm,  $t = 200$  nm,  $h = 150$  nm,  $d = 150$  nm and  $T = 2\mu\text{m}$ . (d) power density profile for the TM mode for  $w = 350$  nm,  $t = 200$  nm,  $h = 150$  nm,  $d = 45$  nm and  $T = 2\mu\text{m}$ . Wavelength of light is  $1550$  nm [18].

#### 4.4. Metal-insulator-metal waveguide

In contrast to the hybrid waveguides, metal-insulator-metal (MIM) structure has a very good modal confinement in cost of a short propagation length. A MIM waveguide is a dielectric slot sandwiched as core between two layers of metal as cladding. The coupling of two SPP's from two metal-dielectric boundaries is the only aspect in common. In the MIM structure, these two SPP's coupled into the central dielectric slot and thus gives rise to a huge field concentration. However, due to the close proximity of the mode with both metal layers, the losses are extremely large. A typical value for propagation length is in the few microns as in the IM case. The most noticeable advantage of the MIM mode is its sub-wavelength size.

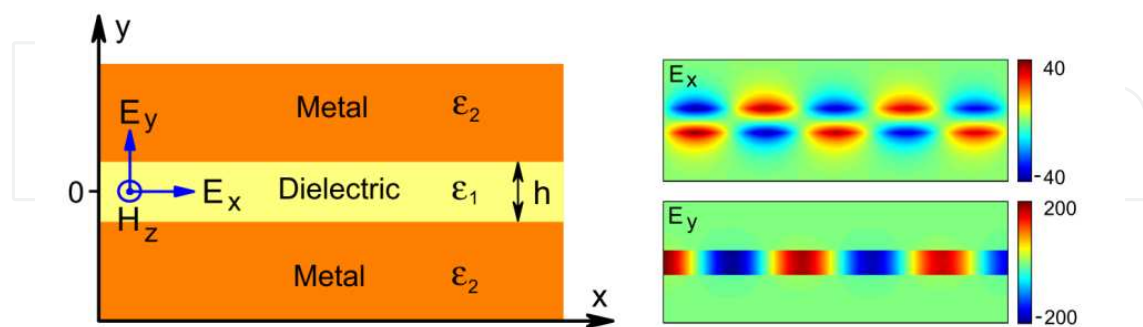


**Figure 6.** Left panel: Schematic of an MIM waveguide with dielectric layer of thickness  $h$  and permittivity  $\epsilon_1$  sandwiched between two metallic layers of permittivity  $\epsilon_2$ . Right panel: Density plots of longitudinal ( $E_x$ ) and transverse ( $E_y$ ) electric fields corresponding to the fundamental anti-symmetric SPP mode [19].

In addition, in the MIM waveguides one could make any sharp geometries or bending regardless of wavelength of the incident optical field [20]. MIM subwavelength plasmonic

waveguide bends and splitters have low loss over a wide frequency range [20]. While metals are naturally lossy, the bounded SP modes of a single insulator-metal interface can propagate over several microns under optical incident fields [21]. In such a geometry, the field skin depth increases exponentially with wavelength in the insulator but is almost constant ( $\sim 25\text{nm}$ ) in the metal for visible and near-infrared excitation frequencies. Not unlike conventional waveguides, these metal-insulator-metal (MIM) structures guide light via the refractive index differential between the core and cladding [21]. However, unlike dielectric slot waveguides, both plasmonic and conventional waveguiding modes can be accessed, depending on transverse core dimensions. MIM waveguides may thus allow optical mode volumes to be reduced to subwavelength scales—with minimal field decay out of the waveguide physical cross section— even for frequencies far from the plasmon resonance.

#### 4.4.1. Dispersion relation for MIM waveguides

The modal analysis of planar multilayer structures can be solved via the vector wave equation under constraint of tangential  $\mathbf{E}$  and normal  $\mathbf{D}$  field continuity [21]. For unpolarized waves in a three-layer symmetric structure, the electromagnetic fields take the form [21]:

$$E(x, z, t) = (E_x \hat{x} + E_y \hat{y} + E_z \hat{z}) e^{i(k_x x - \omega t)} \quad (36)$$

$$B(x, z, t) = (B_x \hat{x} + B_y \hat{y} + B_z \hat{z}) e^{i(k_x x - \omega t)}, \quad (37)$$

with  $E_y$ ,  $B_x$  and  $B_z$  identically zero for transverse magnetic (TM) polarization and  $E_x$ ,  $E_z$  and  $B_y$  identically zero for transverse electric (TE) polarization. Inside the waveguide, the field components may be written as [21]:

$$\begin{aligned} E_x^{in} &= e^{-ik_{z1}z} \pm e^{ik_{z1}z}, \\ E_y^{in} &= 0, \\ E_z^{in} &= \left( \frac{k_x}{k_{z1}} \right) (e^{-ik_{z1}z} \mp e^{ik_{z1}z}), \\ B_x^{in} &= 0, \\ B_y^{in} &= \left( \frac{-\omega \mathcal{E}_1}{ck_x} \right) (e^{-ik_{z1}z} \mp e^{ik_{z1}z}), \\ B_z^{in} &= 0, \end{aligned} \quad (38)$$

for the TM polarization and as:

$$\begin{aligned}
 E_x^{in} &= 0, \\
 E_y^{in} &= e^{-ik_{z1}z} \pm e^{ik_{z1}z}, \\
 B_z^{in} &= 0, \\
 B_x^{in} &= \left( \frac{-k_{z1}c}{\omega} \right) \left( e^{-ik_{z1}z} \mp e^{ik_{z1}z} \right), \\
 B_y^{in} &= 0, \\
 B_z^{in} &= \left( \frac{k_x c}{\omega} \right) \left( e^{-ik_{z1}z} \pm e^{ik_{z1}z} \right),
 \end{aligned} \tag{39}$$

for the TE polarization. Outside the waveguide, the components are given [21]:

$$\begin{aligned}
 E_x^{out} &= \left( e^{-ik_{z1}d/2} \pm e^{ik_{z1}d/2} \right), \\
 E_y^{out} &= 0, \\
 E_z^{out} &= \left( \frac{\epsilon_1 k_x}{\epsilon_2 k_{z1}} \right) \left( e^{-ik_{z1}d/2} \mp e^{ik_{z1}d/2} \right) e^{ik_{z2} \left( z - \frac{d}{2} \right)}, \\
 B_x^{in} &= 0, \\
 B_y^{out} &= \left( \frac{-\omega \epsilon_1}{ck_x} \right) \left( e^{-ik_{z1}d/2} \mp e^{ik_{z1}d/2} \right) e^{ik_{z2} \left( z - \frac{d}{2} \right)}, \\
 B_z^{out} &= 0,
 \end{aligned} \tag{40}$$

for TM polarization and as:

$$\begin{aligned}
 E_x^{out} &= 0, \\
 E_y^{out} &= \left( e^{-ik_{z1}d/2} \pm e^{ik_{z1}d/2} \right) e^{ik_{z2} \left( z - \frac{d}{2} \right)}, \\
 E_z^{out} &= 0, \\
 B_x^{out} &= \left( \frac{-k_{z1}c}{\omega} \right) \left( e^{-ik_{z1}d/2} \mp e^{ik_{z1}d/2} \right) e^{ik_{z2} \left( z - \frac{d}{2} \right)}, \\
 B_y^{out} &= 0, \\
 B_z^{out} &= \left( \frac{k_x c}{\omega} \right) \left( e^{-ik_{z1}d/2} \pm e^{ik_{z1}d/2} \right) e^{ik_{z2} \left( z - \frac{d}{2} \right)},
 \end{aligned} \tag{41}$$

for TE polarization. The in-plane wave vector  $k_x$  is defined by the dispersion relations [21]:

$$L+ : \begin{cases} \varepsilon_1 k_{z2} + \varepsilon_2 k_{z1} \tanh\left(\frac{-ik_{z1}d}{2}\right) = 0 & TM \\ k_{z2} + k_{z1} \tanh\left(\frac{-ik_{z1}d}{2}\right) = 0 & TE \end{cases} \quad (42)$$

$$L- : \begin{cases} \varepsilon_1 k_{z2} + \varepsilon_2 k_{z1} \coth\left(\frac{-ik_{z1}d}{2}\right) = 0 & TM \\ k_{z2} + k_{z1} \coth\left(\frac{-ik_{z1}d}{2}\right) = 0 & TE \end{cases} \quad (43)$$

where  $k_{z2}$  is the momentum conservation:

$$k_{z1,2}^2 = \varepsilon_{1,2} \left(\frac{\omega}{c}\right)^2 - k_x^2 \quad (44)$$

and  $L+$  and  $L-$  denote the antisymmetric and symmetric tangential electric field with respect to the waveguide medium, respectively.

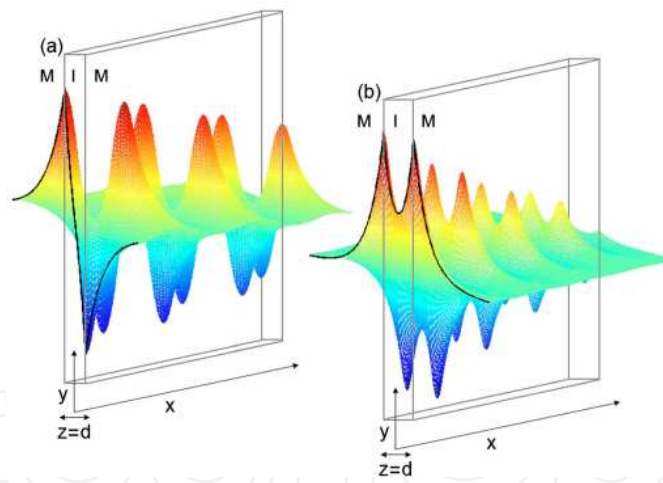


**Figure 7.** Geometry and characteristic tangential ( $x$ ) electric field profiles for MIM slot waveguides; (a) Field antisymmetric mode, (b) Field symmetric mode [21].

In above analysis the structure is centered at  $z=0$  with core thickness  $d$  and wave propagates along the positive  $x$  direction (figure 7). The core (cladding) is composed of material with complex dielectric constant  $\varepsilon_1$  ( $\varepsilon_2$ ). Since continuity of  $E_y$  forbids charge accumulation at the interface, TE surface plasmon waves do not generally exist in planar insulator-metal structures [21]. If SPPs are excited at an insulator-metal interface, electrons in the metal make a surface polarization that leads to a localized electric field. In insulator-metal-insulator (IMI) structures, electrons of the metallic core screen the charge configuration at each interface and maintain a

near-zero (or minimal) field within the waveguide. Therefore, the surface polarizations on both side of the metal film persist in phase and there is no cutoff frequency for any transverse waveguide dimension [21]. In contrast, screening does not occur within the insulator core of MIM waveguides. At each insulator-metal interface, surface polarizations of each side of interface are independent, and therefore SPPs oscillations need not be energy- or wave-vector-matched to each other. As a result, for certain MIM dielectric core thicknesses, interface SPPs may not remain in phase but will exhibit a beating frequency; as transverse core dimensions are increased, “bands” of allowed energies or wave vectors and “gaps” of forbidden energies will be observed [21].

The effective refractive index  $n_{\text{eff}}$  of an MIM waveguide is complex. Its real part controls the guided wavelength  $\lambda_{\text{MIM}}$  and its imaginary part limits the propagation length  $L_{\text{SPP}}$  of SPPs through the relation [19]:

$$n_{\text{eff}} = \frac{\beta}{k} = \frac{\lambda}{\lambda_{\text{MIM}}} + i \frac{\lambda}{4\pi\lambda_{\text{SPP}}} \quad (45)$$

where  $k = 2\pi / \lambda$ ,  $\lambda = 2\pi c_0 / \omega$  and  $c_0$  is the speed of light in vacuum. One can calculate  $\beta$  using the following dispersion relation for the TM-SPP modes [19]:

$$\tanh\left(\frac{ik_1 d}{2}\right) = \left(\frac{\varepsilon_2 k_1}{\varepsilon_1 k_2}\right)^{\pm 1} \quad (46)$$

where the signs  $\pm$  correspond to symmetric and antisymmetric modes. Based on Equation (46), for  $h \ll \lambda$ , an MIM waveguide supports only a single antisymmetric mode that is similar to the fundamental TEM mode of a parallel-plate waveguide with perfect-electric-conductor (PEC) boundaries: The symmetric mode stops to exist because it experiences a cut-off in the reciprocal space [19]. Thus, in the deep subwavelength regime, an MIM waveguide operates as a single-mode plasmonic waveguide. Since this regime is the most interesting from the standpoint of nanophotonics applications, we assume in this chapter that the condition  $h \ll \lambda$  is satisfied and focus on a single-mode plasmonic waveguide [19].

## 5. Modeling of plasmonic MIM waveguides

### 5.1. Challenges in modeling of plasmonics

Numerical simulation and modeling of plasmonic devices involves several challenges specific to plasmonics [22]. The permittivity of metals at optical wavelengths is complex, i.e.  $\varepsilon(\omega) = \varepsilon'(\omega) + i\varepsilon''(\omega)$ , and is a complicated function of frequency [22]. Thus, several simulation techniques which are limited to lossless, non-dispersive materials are not applicable to plasmonic devices [22]. In addition, the dispersion properties of metals have to be approximated by suitable analytical expressions, such as Drude model and Drude-Lorentz model. Furthermore, in surface plasmons propagating along the interface of a metal and an insulator,

the field is confined at the interface, and decays exponentially perpendicular to the direction of propagation. Consequently, for numerical methods based on discretization of the fields, a very fine mesh resolution is required at the metal-dielectric interface [22]. Generally, simulation of plasmonic devices necessitates much finer grid resolution than modeling of low- or high-index-contrast dielectric devices, because of the high localization of the field at metal-dielectric interfaces of plasmonic components. The required grid size depends on the shape and feature size of the modeled plasmonic device, the metallic material used and the operating frequency.

## 5.2. General simulation methods for plasmonic components

Due to the wave nature of the surface plasmon polaritons, most of the simulation methods of plasmonic devices and circuits are the same as the radio frequency approaches; therefore, the most common methods in simulation and modeling of the plasmonics are Finite-Difference Time Domain (FDTD) [23], Finite Element Method (FEM) [24], Transmission Line Method (TLM) [19] and Coupled Mode Theory (CMT) [25]. Each of the methods has its advantages over a specific plasmonic structure, e.g. in order to simulation of a 3D hybrid structure of a ring resonator FDTD or FEM are more convenient and for modeling of a metal-insulator-metal stub filter the accurate and fast approach is TLM. Transient response of a structure may be modelled by simulating electromagnetic pulses in time domain, by methods such as FDTD. The discussion for investigation of the best way to simulate plasmonic waveguides is out of the scope of this chapter; however, some of the most widely used methods are briefly explained.

### 5.2.1. Finite-Difference Time Domain (FDTD)

Finite Difference Time Domain is a common technique in modelling electromagnetics problems [15]. It is considered easy to understand and implement [26]. It is a time-domain method, so depending on the excitation type used, it could cover a wide range of frequencies in a single run, and hence it is usually the method of choice for wideband systems [15]. This method was introduced first by Kane Yee. FDTD does not require the existence of Green's function and directly approximates the differential operators in Maxwell's equations on a grid discretized in time and space. FDTD is an explicit finite difference approach, i.e. no matrix equation is established, stored and solved. The field values at the next time step are given entirely in terms of the field at the current and the previous time steps [15].

FDTD discretizes into unit cells called "Yee cells" [27, 28]. In such Yee cells, Electric Fields are represented by the edges of a cube, where the faces of the cubic cell denote the magnetic field. Given the offset (in space) of the magnetic fields from the electric fields, the values of the field with respect to time are also offset. Time is distributed into small steps, which are corresponding to the amount of time needed for the fields to travel from one Yee cell to the next or less. FDTD method solves the Maxwell's equations using the relationship between the partial time and space derivatives [15]. Yee's algorithm solves both E and H in time and space using the Maxwell's curl equations [26]. The biggest advantage of FDTD is its simplicity of use and fast application.

### 5.2.2. Finite Element Method (FEM)

The finite element method (FEM) is a numerical technique, which approximates the solutions of differential equations [15]. In electromagnetics, FEM generally approaches the solution to the Maxwell's equations in the frequency domain, therefore is usually used with time-harmonic conditions. Furthermore, it is capable of time domain simulations. FEM can be derived using two methods [15]; First, the variational method, which finds a variational functional whose minimum/maximum/stationary point corresponds to the solution of the PDE subject to certain boundary conditions (a brief formulation is given in section 2.7.1). Second method is called the "weak formulation" in the literatures. It works by introducing a weighted residual error to one of the differentials in the PDE form of Maxwell's equations [29] and equating the sum of the error to zero. If the weighting functions are Dirac delta functions, the resulting procedure is similar to finite difference method. If the weighting functions are the basis functions, then the method is called the Galerkin's method [15].

Several commercial software are presented in which simulate the electromagnetic problems based on FEM, such as CST Microwave Studio, COMSOL Multiphysics and ANSYS.

### 5.2.3. Transmission Line Modelling (TLM) method

Transmission Line modelling is one of the time domain techniques that can solve the electromagnetic problems [15]. The concept of impedance and understanding the effects of waveguide discontinuities in terms of lumped circuit elements were crucial in this respect [22]. Although the properties of metals are quite different at optical wavelengths compared to the microwave, designs that are qualitatively similar to their low frequency counterparts have been demonstrated at optical frequencies.

In this method, a unit cell is formed by conceptually filling space with a network of transmission-lines in such a way that the voltage and current give information on the electric and magnetic fields [15]. A node represents the intersection point of the transmission-lines. At each time step, voltage pulses come to the node from each of the transmission-lines. These pulses are then scattered to produce a new set of pulses that become incident on adjacent nodes at the next time step. The relationship between the incident pulses and the scattered pulses is determined by the scattering matrix, which is set to be consistent with Maxwell's equations. Additional elements, such as transmission-line stubs, can be added to the node so that different material properties can be represented [15].

## 6. A case study: Electro-plasmonic switch based on MIM stub filter

### 6.1. Stub filters in MIM plasmonic structures

A stub is one of the key elements in microwave engineering and is employed in various microwave devices to reduce their size [30]. Some research groups have proposed a wavelength filter by using a stub structure in a photonic crystal waveguide [30, 31]. Such a structure may be employed in a plasmon waveguide to perform as a wavelength selective filter.

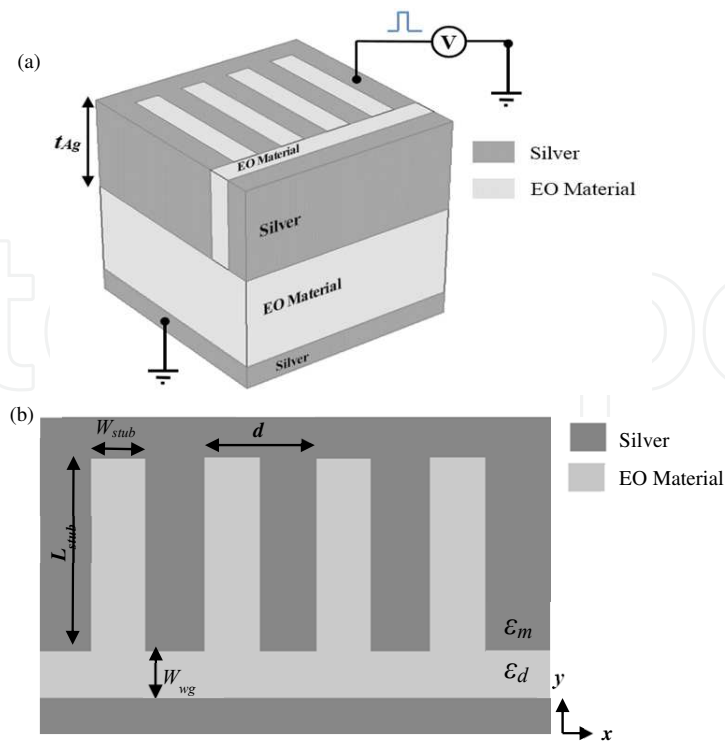


**Figure 8.** (a) three-dimension and (b) two-dimensional schematic depiction of the proposed Electro-Plasmonic switch [34].

Stub filters, also could be employed in order to make plasmonic switches [32-34]. MIM plasmonic waveguide structure helps to shrink the size of a stub filter to nanoscale and the stub structures cause to reduce the threshold voltage of the switch.

## 6.2. MIM Stub filter as a plasmonic switch

Figures 8(a) and 8(b) show the three and two-dimensional schematic of the proposed electro-plasmonic switch based on the MIM structure, respectively [34]. This switch is essentially an MIM stub filter, which comprises of a main waveguide and one or more stub(s) vertically connected to it. Several studies investigated the properties of the stub filters and many researches used their filtering characteristics [19, 35-36].

The width of the waveguide and stubs, the length of the stubs and the displacement between them, and the refractive index of the core adjust the properties of the stub filter [19]. Any change in these factors will change the transfer function of the filter; therefore, one can control the transmittance valley or peak of the filter with a change in above parameters. Thus, through altering the refractive index of the core by applying an electric field to an EO material one could have an EO switch. In an MIM structure, the metal cladding boosts the electro optic effect in the core; subsequently, it decreases the threshold voltage of the switch.

Here, it is supposed that the entire of the switch filled with an EO material known as 4-dimethyl-amino-Nmethyl-4-stilbazolium tosylate (DAST) as the core, with a linear refractive index of  $n_d = 2.2$  and a large EO coefficient ( $dn/dE = 3.41 \text{ nm/V}$ ) [37].

Due to the low losses for the surface plasmons propagation, here silver is selected as the metal cladding of the waveguide [38]. In all simulations, the Drude-Lorentz model of the silver is utilized in order to obtain accurate results. A seven-pole Drude-Lorentz model is used in the wavelength range from 0.4μm to 2μm [19]:

$$\epsilon_m(\omega) = 1 - \frac{\omega_p^2}{\omega(\omega + i\gamma)} + \sum_{n=1}^5 \frac{f_n \omega_n^2}{\omega_n^2 - \omega^2 - i\omega\gamma_n} \quad (47)$$

where,  $\omega_p = 2002.6$  THz is the bulk plasma frequency of silver and  $\gamma = 11.61$  THz is a damping constant [19]. Table 1 listed the other parameters. In addition, we used an analytical expression to calculate of the effective index of the fundamental TM<sub>0</sub> mode in the entire of the device [39]:

$$n_{eff} = \sqrt{\epsilon_d} \left( 1 + \frac{\lambda}{\pi w \sqrt{-\epsilon_m}} \sqrt{1 + \frac{\epsilon_d}{-\epsilon_m}} \right)^{\frac{1}{2}} \quad (48)$$

where,  $w$  is the width of the waveguide and  $\epsilon_d = n_d^2$ . The real and imaginary parts of the effective index for  $w = 50$ nm over the wavelength range from 0.4 to 2μm is depicted in figure 9.

n	$\omega_n$ (THz)	$\gamma_n$ (THz)	$f_n$
1	197.3	939.62	7.9247
2	1083.5	109.29	0.5013
3	1979.1	15.71	0.0133
4	4392.5	221.49	0.8266
5	9812.1	584.91	1.1133

**Table 1.** Parameters of the Drude-Lorentz Model for Silver [19].

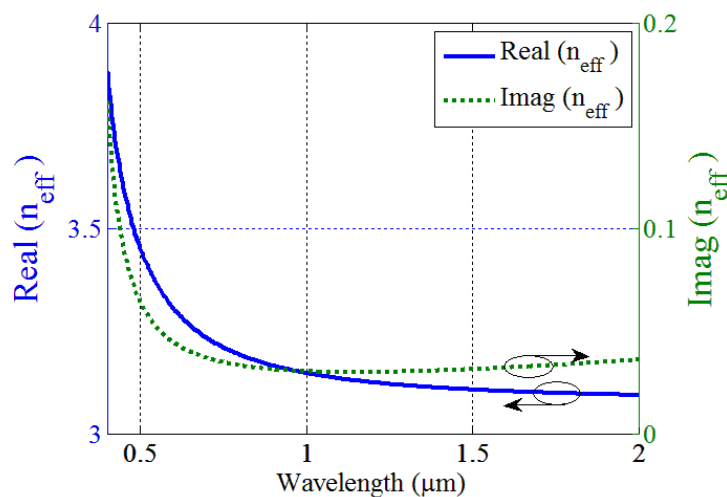


**Figure 9.** The real and imaginary part of the effective refractive index for MIM waveguide with the linear refractive index  $n_d = 2.2$  and  $W_{wg} = 50$ nm [34].

### 6.2.1. Modeling of the device using TLM

The Transmission Line Method (TLM) helps to study the operation of the MIM stub filters more accurately and faster [35], in comparison to other methods. In this method, we convert the plasmonic MIM structure in figure 10a to an equivalent circuit diagram (see figure 10b). This equivalent circuit is formed by a parallel connection of the characteristic impedance of an infinite MIM waveguides ( $Z_{MIM}$ ) and the characteristic impedance of a finite and  $L_{spp}$  is the propagation length of the SPPs (equation (35)). The length of the stubs is the key point of the design of the stub filter and the electro-plasmonic switch [34]. Knowing that small increase in the real part of the refractive index leads to a red-shift in the transmittance spectrum of the filter, the transmission of the filter at wavelength  $\lambda=1550\text{nm}$  must be on the edge of a change, a falling edge of the magnitude for normally ON and a rising edge for normally OFF switch. Figure 11 shows the transmission of a typical 4-stub filter for different length of the stubs. The transmittance is defined as  $T=P_{out}/P_{in}$  and is calculated using Transmission Line Method [35]. In the computation of the spectrum, the width of the main waveguide and the width of the stubs has the same value  $W_{wg}=W_{stub}=50\text{nm}$ , the distances between stubs is  $d=100\text{nm}$  and the thickness of the silver layer (or the depth of the structure) is  $t_{Ag}=200\text{nm}$ .

MIM waveguide ( $Z_S$ ) terminated by  $Z_L$  accounts for reflection of the SPPs from the stub [19]:

$$Z_S = Z_{MIM} = \frac{\beta(w)w}{\omega\epsilon_d\epsilon_m} \quad (49)$$

$$Z_L = \sqrt{\frac{\epsilon_m}{\epsilon_d}} \times Z_S \quad (50)$$

$\beta(w)$  is the complex-valued propagation constant and describes the properties of the MIM waveguide. The circuit diagram in figure 10b may be modified to an equivalent form as shown in figure 10c by replacing  $Z_{MIM}$  and  $Z_S$  by an effective impedance ( $Z_{stub}$ ). The value of  $Z_{stub}$  can be found from transmission-line theory and is given by [19]:

$$Z_{stub} = Z_S \frac{Z_L - iZ_S \tan(\beta(w)L_{stub})}{Z_S - iZ_L \tan(\beta(w)L_{stub})} \quad (51)$$

Now, we calculate the transmission spectra of an MIM stub filter with  $N$  identical stubs set apart by a distance  $d$ , the length of the stubs  $L_{stub}$ , the width of waveguide and stubs  $W_{wg} = W_{stub} = w$  [39]:

$$T = \left( P_+^{N-1} Q_+ - P_-^{N-1} Q_- \right)^{-2} \exp\left(-\frac{L}{L_{spp}}\right) \quad (52)$$

where

$$P_{\pm} = \frac{1}{2} \left[ 1 + \frac{Z_{MIM}}{2Z_{stub}} + \left( 1 - \frac{Z_{MIM}}{2Z_{stub}} \right) \exp(2i\beta d) \pm R \right],$$

$$Q_{\pm} = \frac{1}{2R} \left( \left( 1 + \frac{Z_{MIM}}{2Z_{stub}} \right)^2 - \left[ 1 + \left( \frac{Z_{MIM}}{2Z_{stub}} \right)^2 \right] \exp(2i\beta d) \right) \pm \frac{1}{2} \left( 1 + \frac{Z_{MIM}}{2Z_{stub}} \right)$$

$$R = \left\{ \left[ 1 + \frac{Z_{MIM}}{2Z_{stub}} + \left( 1 - \frac{Z_{MIM}}{2Z_{stub}} \right) \exp(2i\beta d) \right]^2 - 4 \exp(2i\beta d) \right\}^{\frac{1}{2}},$$

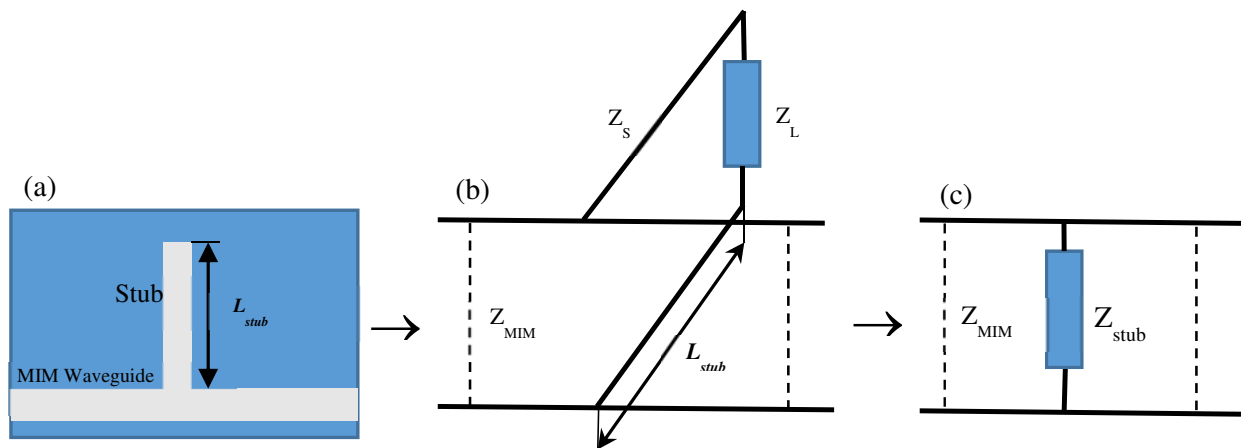


**Figure 10.** The diagram of an MIM waveguide with a single stub coupled perpendicularly to the waveguide axis. (b) The corresponding transmission-line representation. (c) The simplified circuit model.  $Z_{MIM}$  and  $Z_s$  correspond to the characteristic impedance of the MIM waveguide and the stub, respectively,  $Z_L$  accounts for reflection of the SPPs from the stub end and  $Z_{stub}$  is the effective stub impedance [19].

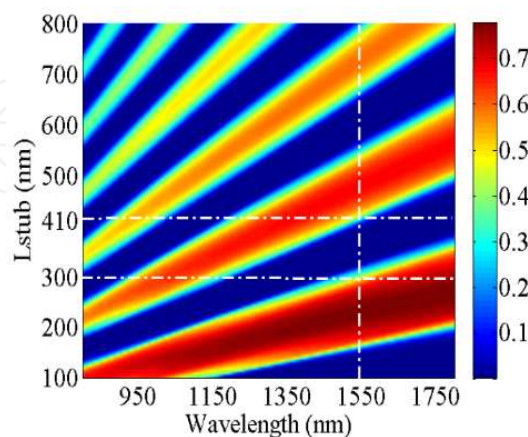


**Figure 11.** The transmittance spectra of the 4-stub filter for different length of the stubs. The crossing points of the dashed-lines show the transmittance values for  $L_{stub}=300\text{nm}$  and  $L_{stub}=410\text{nm}$  when  $\lambda = 1550\text{nm}$ . By a red-shift in the spectrum, the magnitude of the transmittance rises at the point a while falls at the point b [34].

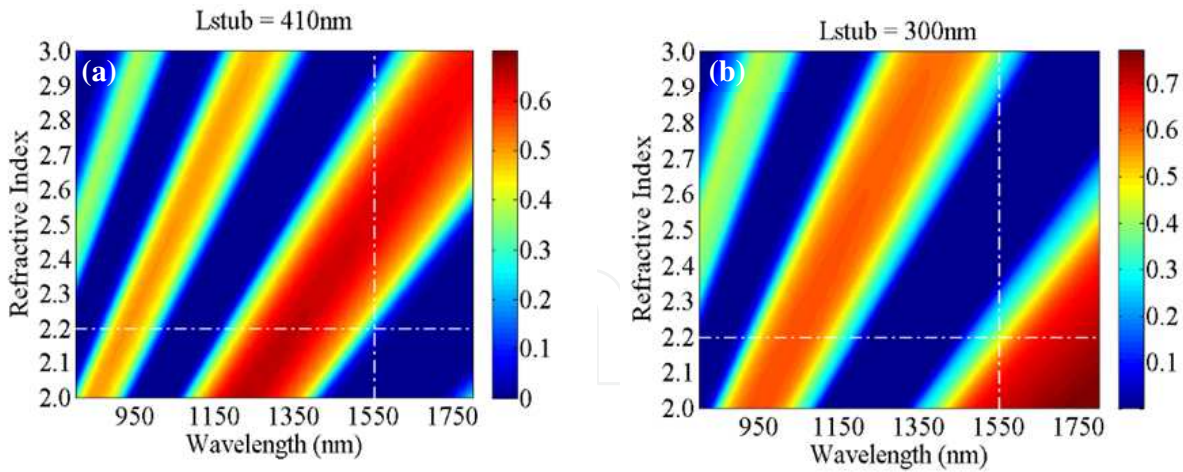


**Figure 12.** The transmittance spectra of the 4-stub filter for different refractive index with (a)  $L_{\text{stub}} = 410\text{nm}$ , and (b)  $L_{\text{stub}} = 300\text{nm}$ ; the crossing of the dashed-lines indicate the transmittance of the filter with the correspond  $L_{\text{stub}}$ . Increment in the refractive index at 1550nm leads to (a) rise, (b) fall the magnitude of the transmittance [34].

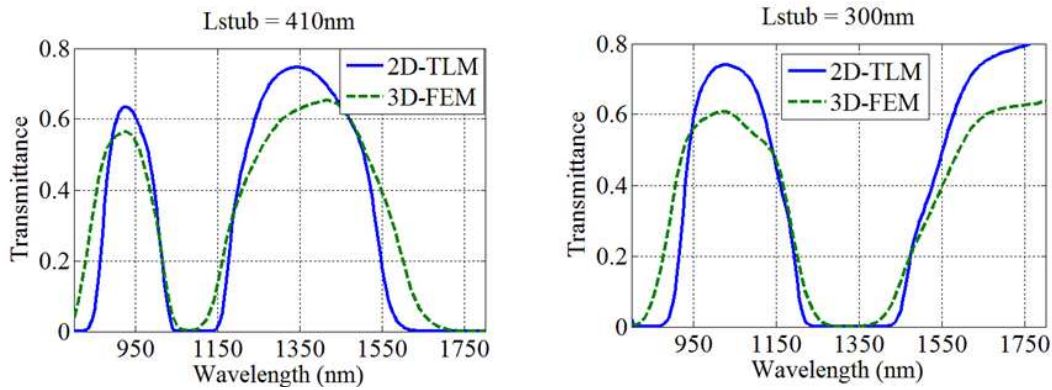


**Figure 13.** The transmittance spectra of the 4-stub filter with (a)  $L_{\text{stub}} = 410\text{nm}$ , and (b)  $L_{\text{stub}} = 300\text{nm}$ ; in the calculation of the spectrums, 2D-TLM and 3D-FEM methods are used which show an acceptable conformity [34].

According to figure 11, by selecting the stub  $L_{\text{stub}} = 300\text{nm}$  (point b) or  $L_{\text{stub}} = 410\text{nm}$  (point a) at the communication wavelength  $\lambda = 1550\text{nm}$ , the normal state of the switch would be ON or OFF, respectively. Slightly increment in the refractive index turns the switch OFF or ON, depending on the length of stubs ( $L_{\text{stub}} = 300\text{nm}$  or  $L_{\text{stub}} = 410\text{nm}$ , respectively). Figures 12a and 12b show the spectrum of the switch versus the refractive index for  $L_{\text{stub}} = 300\text{nm}$  and  $L_{\text{stub}} = 410\text{nm}$ , respectively. Figures 13a and 13b show the transmission spectrum for  $L_{\text{stub}} = 410\text{nm}$  and  $L_{\text{stub}} = 300\text{nm}$  and shows reasonable accuracy of three-dimensional FEM simulations [34]. These figures admit the red-shift effect on the ON/OFF status of the switch. As shown in figure 8, the silver cladding is connected to the voltage  $V$  and therefore the electric field surrounds the main waveguide and all the stubs. The relation between applied voltages and the refractive index of EO material is expressed using equation [37]:

$$n = n_0 + \frac{dn}{dE} \left( \frac{V}{w} \right) \quad (53)$$

where  $n_0$  is the linear refractive index of the EO material that equals 2.2,  $V$  is the applied voltage, and  $w$  is the width of waveguides and stubs [34]. The applied electric field alters the linear refractive index of the switch and as a result causes the red-shift. Figures 14a-d demonstrate the distribution of the optical field in the structure of the electro-plasmonic switch. In figures 14a and 14c the applied voltage is 0V and corresponds to the normal-state of both switches, while figures 14b and 14d show the electro-optic switch when the voltage is applied to the structure. The applied electric field changes the refractive index of the EO material; therefore, the optical field reflected back to the input port. Figure 15 depicts the transmittance of the normally ON and normally OFF switch as a function of the applied voltage at the wavelength 1550nm. As can be seen, the threshold voltage for switching is 10V [34].

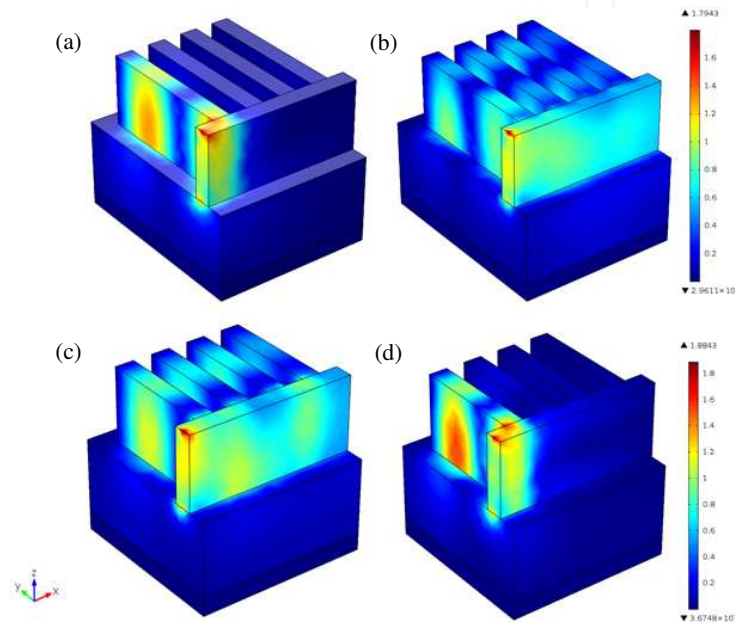


**Figure 14.** The distribution of the optical field in the structure of the electro-optic switch for  $L_{\text{stub}}=410\text{nm}$  when (a)  $V = 0\text{V}$  (b)  $V = 10\text{V}$  and  $L_{\text{stub}}=300\text{nm}$  when (c)  $V = 0\text{V}$  (d)  $V = 10\text{V}$  [34].

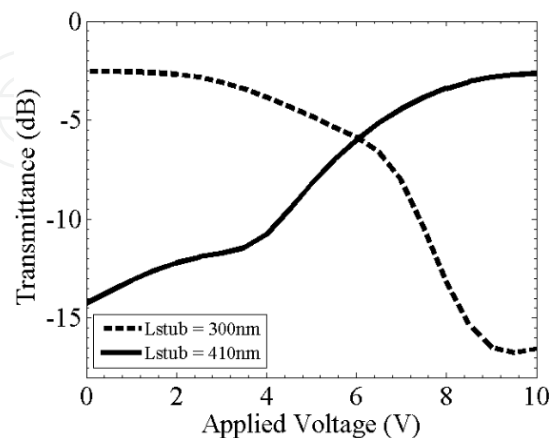


**Figure 15.** The transmittance of the proposed electro-optic switch versus the applied voltage at the telecom wavelength 1550nm; the solid and dashed line corresponds to EO switch with the  $L_{\text{stub}}=410\text{nm}$  (Normally OFF) and the  $L_{\text{stub}}=300\text{nm}$  (Normally ON), respectively [34].

## Author details

Hassan Kaatuzian\* and Ahmad Naseri Taheri

\*Address all correspondence to: hsnkato@aut.ac.ir

Photonics Research Lab., Amirkabir university of Technology, Iran

## References

- [1] Atwater Harry, The promise of Plasmonics, Scientific American, April 2007.
- [2] L. Rayleigh. Phil. Mag., 47, 1899.
- [3] J. C. Maxwell Garnett. Colours in metal glasses and in metallic films. Philosophical Transactions of the Royal Society of London, 203, 1904.
- [4] G. Mie. Beitrage zur optik truber medien, speziell kolloidaler metall°osungen. Annalen Der Physik, 25(3):377–445, 1908.
- [5] R. H. Ritchie. Plasma losses by fast electrons in thin films. Physical Review, 106, 1957.
- [6] A. Otto. Excitation of nonradiative surface plasma waves in silver by the method of frustrated total reflection. Zeitschrift fur Physik, 1968.
- [7] E. Kretschmann and H. Raether. Radiative decay of non-radiative surface plasmons excited by light. Zeitschrift fur Naturforschung, 23A, 1968.
- [8] M Fleischmann, P.J. Hendra, and A.J. McQuillan. Raman spectra of pyridine adsorbed at a silver electrode. Chemical Physics Letters, 26, 1974.
- [9] Kaatuzian Hassan, "Quantum Photonics, A Theory for Attosecond Optics", AKU Press, ISBN: 978-964-463-273-0, 2012.
- [10] D. K. Gramotnev and S. I. Bozhevolnyi, "Plasmonics beyond the diffraction limit," Nat.Photon. 4, 83-91 (2010).
- [11] Zia, R., Schuller, J. A., Chandran, A., Brongersma, M. L.: Plasmonics: the next chip-scale technology, Materials Today 9, 20 (2006).
- [12] Sweatlock L.A., Plasmonics: Numerical Methods and Device Applications. PhD Thesis. California Institute of Technology. 2008.
- [13] Kaatuzian Hassan, "Photonics, vol-1", AKU Press, ISBN: 964-463-271-0, 2008.
- [14] Maier S. A. Plasmonics: Fundamentals And Applications. Springer. 2007.
- [15] Ahmet Arca. The design and optimisation of nanophotonic devices using the Finite Element Method. PhD Thesis. University of Nottingham. 2010.

- [16] A. Kumar, J. Gosciniak, V. S. Volkov, S. Papaioannou, D. Kalavrouziotis, K. Vyrsokinos, J.-C. Weeber, et al., Dielectric-loaded plasmonic waveguide components: going practical, *Laser Photon. Rev.* 7 (6), pp. 938–951, 2013. doi:10.1002/lpor.201200113
- [17] T. Holmgaard, J. Gosciniak, and S. I. Bozhevolnyi, “Long-range dielectric-loaded surface plasmon-polariton waveguides,” *Opt. Express* 18(22), 23009–23015 (2010).
- [18] Muhammad Zulfiker Alam, *Hybrid Plasmonic Waveguides: Theory and Applications*. PhD Thesis. University of Toronto. 2012.
- [19] Pannipitiya, A., Rukhlenko, I. D., Premaratne, M., Hattori, H. T., Agrawal, G. P.: Improved transmission model for metal-dielectric-metal plasmonic waveguides with stub structure, *Opt. Express*, Vol. 18, No. 6, 6191 (2010).
- [20] G. Veronis, and S. H. Fan, “Bends and splitters in metal-dielectric-metal subwavelength plasmonic waveguides,” *Appl. Phys. Lett.* 87(13), 131102 (2005).
- [21] J. A. Dionne, L. A. Sweatlock, and H. A. Atwater. Plasmon slot waveguides: Towards chip-scale propagation with subwavelength-scale localization. *Physical Review B* 73, 035407, 2006.
- [22] G. Veronis, S. E. Kocabaş, D. A. B. Miller, and S. Fan, “ Modeling of plasmonic waveguide components and networks, ” *J. Comput. Theor. Nanosci.* 6, 1808 – 1826 (2009).
- [23] Y. Zhao, and Y. Hao, “Finite-difference time-domain study of guided modes in nano-plasmonic waveguides,”*IEEE Trans. Antennas Propag.* 55, 3070-3077 (2007).
- [24] J. M. McMahon, A.-I. Henry, K. L. Wustholz, M. J. Natan, R. G. Freeman, R. P. Van Duyne, and G. C. Schatz, “Gold nanoparticle dimer plasmonics: finite element method calculations of the electromagnetic enhancement to surface-enhanced Raman spectroscopy,” *Anal. Bioanal. Chem.* 394(7), 1819–1825 (2009).
- [25] W.-P. Huang, “Coupled-mode theory for optical waveguides: an overview,” *J. Opt. Soc. Am. A* 11, 963-983 (1994).
- [26] A. Taflove and S. C. Hagness. *Computational Electrodynamics: the finite-difference time domain method*. Artech House, Norwood MA, 2000.
- [27] Yee Kane S., “Numerical Solution of Initial Boundary Value Problems Involving Maxwells Equations in Isotropic Media,” *IEEE T. Antenn. Propag.*, vol. 14, 1966.
- [28] A. Taflove, “Application of finite-difference time-domain method to sinusoidal steady-state electromagnetic-penetration problems,” *IEEE Transactions on electromagnetic compatibility*, vol. EMC-22, no. 3, 1980.
- [29] D. B. Davidson, *Computational Electromagnetics for RF and Microwave Engineering*. Cambridge University Press, 2005.

- [30] Y. Matsuzaki, T. Okamoto, M. Haraguchi, M. Fukui, and M. Nakagaki, "Characteristics of gap plasmon waveguide with stub structures," *Opt. Express* 16, 16314-16325 (2008).
- [31] K. Ogusu and K. Takayama, "Transmission characteristics of photonic crystal waveguides with stubs and their application to optical filters," *Opt. Lett.* 32, 2185-2187 (2007).
- [32] Min, C., Veronis, G.: Absorption switches in metal-dielectric-metal plasmonic waveguides, *Opt. Express*, Vol 17, No. 13, 10757 (2009).
- [33] Naseri Taheri A. and Kaatuzian H. Design and simulation of a nanoscale electroplasmonic  $1 \times 2$  switch based on asymmetric metal – insulator – metal stub filters, Vol. 53, No. 27, *Applied Optics*, 2014.
- [34] Naseri Taheri A. and Kaatuzian H. Numerical Investigation of a Nano-Scale Electro-Plasmonic Switch Based on Metal-Insulator-Metal Stub Filter. *Opt Quant Electron.* Springer 2014.
- [35] Liu, J., Fang, G., Zhao, G., Zhang, Y., Liu S.: Surface plasmon reflector based on serial stub structure, *Opt. Express*, 17, 20134 (2009).
- [36] Park, J., Kim, H., Lee, B.: High order plasmonic Bragg reflection in the metal-insulator-metal waveguide Bragg grating, *Opt. Express*, Vol. 16, No. 1, 413 (2008).
- [37] Jin, Z. Y., Guange, H. X., Xian, M.: A Surface Plasmon Polariton Electro-Optic Switch Based on a Metal-Insulator-Metal Structure with a Strip Waveguide and Two Side-Coupled Cavities, *Chin. Phys. Lett.*, Vol. 29, No. 6, 064214, 2012.
- [38] Nielsen, M., Elezzabi, A.: Frequency-selective 3-D integration of nanoplasmonic circuits on a Si platform, *Opt. Express*, Vol. 20, No. 8, 8592 (2012).
- [39] Collin, S., Pardo, F., Pelouard, J.: Waveguiding in nanoscale metallic apertures, *Opt. Express*, Vol. 15, No. 7, 4310, (2007).

IntechOpen